 FDMP, vol.7, no.4, pp.403-418, 2011

Dispersion of Fish Eggs under Undular and Breaking Tidal Bores

H. Chanson[1] **and K.K. Tan**[2]

Abstract: A tidal bore is a wall of water propagating upstream as the tidal flow turns to rising into an estuary with a tidal range larger than 5 to 6 m and the bathymetry that amplifies the tidal wave. The bore front is a shock characterised by a singularity of the free-surface and pressure and velocity fields. This study aims to characterise the impact of tidal bores on the turbulent dispersion of fish eggs. Some physical modelling was performed based upon a Froude similitude and the tracking of plastic beads acting as fish egg proxies was conducted under controlled flow conditions with both undular and breaking tidal bores. The physical experiments highlighted some large-scale coherent structures generated beneath the bore front and advected behind. The vortical structures were responsible for some selective longitudinal dispersion of fish eggs depending upon the eggs' relative density.

Keywords: Tidal bores, Turbulent dispersion, Fish egg dispersion, Mixing, Physical modelling.

1 Introduction

A tidal bore forms during spring tide conditions when the tidal range exceeds 5 to 6 m and the flood tide is confined to a narrow funnelled estuary (Lighthill 1978, Chanson 2011). A bore is a wall of water propagating upstream as the tidal flow turns to rising. When the ocean level at the river mouth rises with time during the early flood tide, the leading edge of the tidal wave becomes steeper and steeper, until it forms an abrupt front that is the tidal bore (Fig. 1). The bore is a powerful natural phenomenon, attracting tourists, kayakers and surfers (Fig. 1a) and causing a strong mixing of the waters. However, the tidal bore processes remain poorly understood today because of a lack of detailed field observations and comprehensive studies (Simpson et al. 2004, Wolanski et al. 2004).

[1] University of Queensland, School of Civil Engineering, Brisbane QLD 4072, Australia.
[2] University of Queensland, School of Civil Engineering, Brisbane QLD 4072, Australia.

(A) Undular tidal bore of the Dordogne River on 30 Sept 2008 afternoon - The kayakers rode the 2nd wave crest while the surfer was ahead of the 3rd wave crest

(B) Sélune river tidal bore on 19 Sept. 2008 morning - Bore propagating from left to right - Note the breaking front in the foreground and the undulations in the deeper section

Figure 1: Photographs of tidal bores

During the 1990s, a team of biologists observed some unusual longitudinal dispersion of fish eggs in a tidal bore affected estuary (Tull 1997, Rulifson and Tull 1999). They studied the populations of striped bass (*Marone saxatilis*) fish eggs in the tidal bore-dominated Shubenacadie-Stewiacke estuarine zone in the Bay of Fundy, Nova Scotia. Their results suggested that the eggs were retained in the estuarine zone by the tidal bore actions, although the large-scale turbulence was responsible for some longitudinal dispersion of fish eggs reducing the impact of their predators (Morris et al. 2003).

It is the aim of this study to characterise the tidal bore induced mixing and longitudinal dispersion of fish eggs. This was achieved through some physical modelling performed under controlled flow conditions based upon a Froude dynamic similarity. Plastic beads were used as proxy of fish eggs and their tracking was conducted during the passage of tidal bores. The results gave a detailed description of the particle mixing processes, and provided a physical understanding of the turbulent dispersion of particulates such as fish eggs.

2 Physical modelling, experimental facility and instrumentation

2.1 Presentation

The analytical and numerical studies of fish egg dispersion in tidal bores are difficult considering the large number of relevant equations and the flow unsteadiness. While relatively simpler, experimental investigations require the selection of an adequate similitude. In any study of particle dispersion in turbulent flows, the relevant parameters needed for any dimensional analysis include the fluid properties and physical constants, the channel geometry and inflow conditions, and particle characteristics. For a tidal bore propagating in a horizontal, rectangular channel, a simplified dimensional analysis yields:

$$u, v, w = F_1\left(t, S, shape, \alpha, U, d_o, V_o, B, g, \rho, \mu, \sigma ...\right) \quad (1)$$

where u, v, w are respectively the longitudinal, transverse and vertical particle velocity components at a time t, S is the relative density of the particle of a given shape and α is the particle loading, U is the tidal bore celerity, d_o is the initial depth, V_o is the initial flow velocity (Fig. 2), B is the channel width, g is the gravity acceleration, ρ and μ are the water density and dynamic viscosity respectively, and σ is the surface tension. In Equation (1), the particle trajectory properties (left handside terms) at a time t are expressed as functions of the particle characteristics, tidal bore properties, initial flow properties, channel geometry and fluid properties. In addition, the biochemical properties of the water solution may be considered especially in natural estuarine systems.

For a tidal bore, the relevant characteristic length scale is the initial flow depth d_o and the relevant Froude number is the tidal bore Froude number $Fr = (V_o + U)/\sqrt{g\,d_o}$ (Hornung et al. 1995, Chanson 2011). For spherical particles, Equation (1) may be rewritten in dimensionless terms:

$$\frac{u}{V_o}, \frac{v}{V_o}, \frac{w}{V_o} = F_2\left(t\sqrt{\frac{g}{d_1}}, S, \frac{D}{d_o}, \alpha, \frac{V_o+U}{\sqrt{g\,d_o}}, \rho \times \frac{(V_o+U)\,d_o}{\mu}, \frac{B}{d_o}, \frac{g\,\mu^4}{\rho\,\sigma^3}, ...\right) \quad (2)$$

where D is the particle diameter. In Equation (2) right handside, the fifth and sixth terms are the tidal bore Froude and Reynolds numbers respectively, and the eighth term is the Morton number which is a function only of fluid properties and gravity constant. For the same fluids (air and water) in both model and prototype, the Morton number becomes a constant.

In free-surface flows including tidal bores, the gravity effects are important and a Froude dynamic similarity is commonly used (Lighthill 1978). But the turbulent mixing processes are dominated by viscous forces implying the needs for a Reynolds similitude. For geometrically-similar models, it is impossible to satisfy simultaneously all the similarities. In practice, the physical studies are based upon a Froude similitude including the present study, but no systematic study was conducted to date to assess the scale effects affecting the turbulent mixing in tidal bores. It is worth noting that the above analysis (Eq. (2)) does not account for the physio-chemical properties of the water nor time-evolution of the particle properties (e.g. during fish egg fertilisation).

2.2 Experimental channel

The experiments were performed in a 12 m long 0.5 m wide rectangular channel (Fig. 2). The flume was horizontal and made of smooth PVC bed and glass walls. The waters were supplied by a constant head tank feeding a large intake basin (2.1 m long, 1.1 m wide, 1.1 m deep) leading to the test section through a bed and sidewall convergent. A radial gate was located at the channel downstream end (x = 11.9 m) where x is the longitudinal distance from the channel test section upstream end and that gate was used to control the initial water depth; its position did not change during an experiment. A fast-closing tainter gate was also located at x = 11.15 m and the gate was closed rapidly (completely or partially) to generate the tidal bore propagating upstream in the channel.

2.3 Instrumentation

The steady flow rate Q was measured with two orifice meters that were designed based upon the British Standards (1943). In steady flows, the water depths were

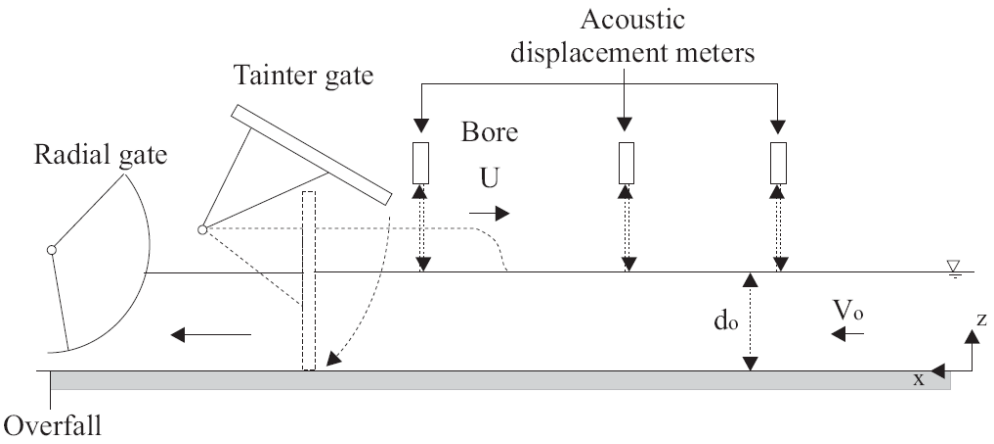

Figure 2: Sketch of the laboratory channel test section

measured using rail mounted pointer gauges. The bore propagation was studied with a series of acoustic displacement meters Microsonic™ Mic+25/IU/TC located along the channel between x = 10.8 and 4 m, and above the water surface (Fig. 2). Between x = 5.65 and 4.85 m, some free-surface observations and particle trajectories were recorded using a digital video camera Panasonic$_{TM}$ NV-GS300 (30 fps) as well as digital cameras.

2.4 Generation of the tidal bore

The experimental geometry and configuration were chosen to have an initially steady open channel flow with a discharge Q ranging from 0.013 to 0.058 m^3s^{-1} (Table 1). The steady flow rate was kept constant for the duration of each experiment. The opening of the downstream radial gate (Fig. 2) controlled the initial steady flow depth d_o and velocity V_o. It was kept constant for a given experiment, and the initial flow depths ranged from about 0.05 to 0.20 m for each steady flow rate.

The tidal bore was generated by the rapid closure of the downstream tainter gate (Fig. 2). The gate operation resulted in a closure time less than 0.15 s. After the rapid closure, the bore propagated upstream (Fig. 3) and each run was stopped when the tidal bore front reached the upstream intake structure ($x < 0$) to avoid any wave reflection in the test section.

The experimental flow conditions are summarised in Table 1 where they are compared with earlier similar studies.

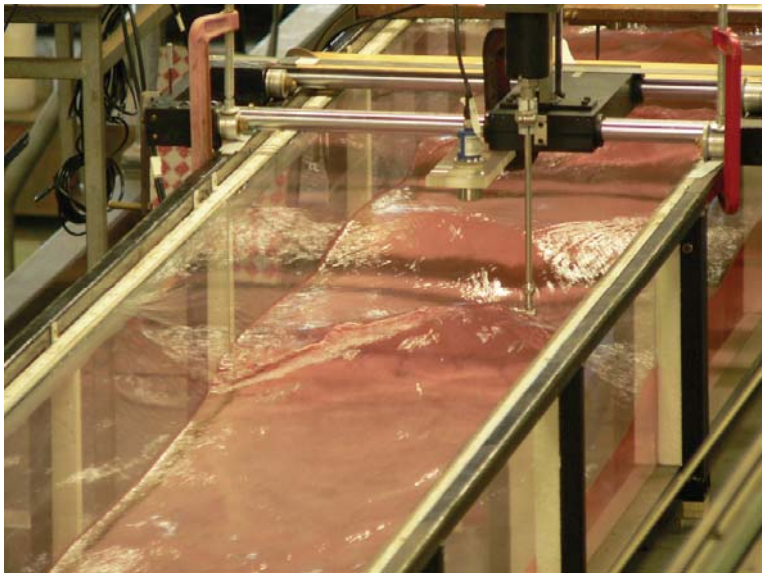

(A) Undular tidal bore (Fr = 1.4, Q = 0.040 m^3s^{-1}, d_o = 0.08 m)

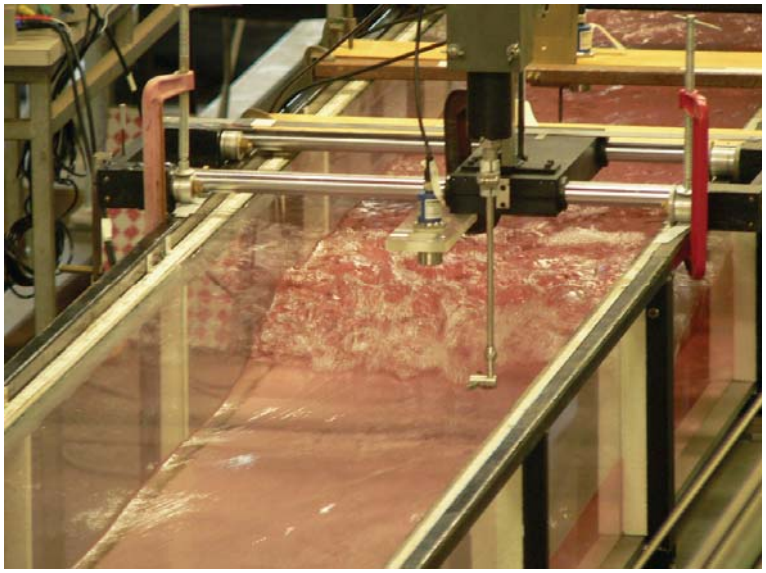

(B) Breaking tidal bore (Fr = 1.7, Q = 0.040 m^3s^{-1}, d_o = 0.079 m)

Figure 3: Photographs of laboratory tidal bores - Looking downstream at the incoming bore

Table 1: Experimental investigations of tidal bores

Ref.	Q	d_o	U	Fr	Comment
	m^3s^{-1}	m	ms^{-1}		
Hornung et al. (1995)	0	–	–	1.5 to 6	Smooth bed.
Koch & Chanson (2009)	0.040	0.079	0.14 to 0.68	1.3 to 2.0	B = 0.5 m. Smooth bed.
Chanson (2010)	0.058	0.14	0.5 to 0.9	1.1 to 1.5	B = 0.5 m. Smooth & rough beds.
Present study	0.013 to 0.058	0.0505 to 0.196	0.33 to 1.19	1.01 to 1.7	B = 0.5 m. Smooth bed.
	0.013	0.0775	0.67	1.15	Particle trajectory
		0.0505	0.55	1.51	experiments

2.5 Particle trajectory experiments

The fish egg substitutes were spherical-shaped beads with an average diameter D = 3.72 mm. Their relative density was deduced from the particle fall velocity measured in a 2 m high, 0.10 m diameter perspex water column. The experimental data yielded a particle fall velocity w_s = 0.047 $\pm$0.012 m/s corresponding to a relative density S = 1.037 $\pm$0.012. The particle diameter and density were close to those of striped bass fish eggs. Tull (1997) measured typical striped bass fish egg diameters of about 4 mm with a specific density S between 1.0016 and 1.0066 depending upon their stages of development. That is, S = 1.0 16 for unfertilised water hardened eggs, S = 1.0029 for fertilised eggs less than 10 hours old, and S = 1.0060 for the heaviest eggs in the final stages of development (Rulifson and Tull 1999). For comparison, the present experiments were conducted in freshwater (S = 1), while the estuarine waters are brackish with a relative density ranging from that of freshwater in the upper extent of the estuary to that of seawater (S = 1.024) at the river mouth.

For an initial discharge Q = 0.013 m^3s^{-1}, the turbulent dispersion of fish egg proxy particles was systematically recorded between x = 5.65 and 4.85 m with an undular bore and a breaking bore (Table 1). The particles were injected on the centreline at the channel upstream end and they were advected downstream by the initially steady flow. Their mixing in the tidal bore front was recorded through the glass

sidewalls using the video camera. The particle loading was very low since no more than 3 to 5 particles were used per experiment.

3 Basic flow patterns

Some visual observations and free-surface measurements were conducted for a range of flow conditions with initially-steady subcritical open channel flow (Table 1). Several flow patterns were observed depending upon the tidal bore Froude number $Fr = (V_o + U)/\sqrt{g\,d_o}$ with d_o the initial flow depth, V_o the initial flow velocity positive downstream, g the gravity acceleration and U the surge front celerity for an observer standing on the bank and positive upstream. Fr is the tidal bore Froude number defined in the system of co-ordinates in translation with the tidal bore. Figure 3 illustrates two examples of laboratory tidal bores.

For a Froude number between unity and 1.5 to 1.6, the tidal bore was undular: that is, the wave front was followed by a train of secondary, quasi-periodic waves called undulations or whelps (Fig. 1A & 3A). For larger Froude numbers, a breaking bore was observed (Fig. 1B & 3B). The basic flow pattern observations were consistent with the earlier findings of Favre (1935), Benet and Cunge (1971), Treske (1994) and Hornung et al. (1995). The undular bore had a smooth, quasi-two-dimensional free-surface profile for Fr < 1.2 to 1.25. For 1.2 to 1.25 < Fr, some slight cross-waves (shock waves) were observed, starting next to the sidewalls upstream of the first wave crest and intersecting next to the first crest on the channel centreline. These cross-waves are seen in Figure 3A. For 1.35 < Fr < 1.5 to 1.6, some slight wave breaking was observed at the bore front, and the secondary waves were flatter. The findings were comparable to those of earlier studies (Koch and Chanson 2009, Chanson 2010). For the largest bore Froude numbers (i.e. Fr > 1.5 to 1.6), the bore had a marked roller, and appeared to be quasi-two-dimensional (Fig. 3B). Behind the roller, the free-surface was about horizontal although large free-surface fluctuations were observed. Some air entrainment and intense turbulent mixing was observed in the bore roller.

The free-surface flow patterns were basically independent of the initially steady flow Froude number $V_o/\sqrt{g\,d_o}$, and an earlier study showed that these were basically independent of the bed roughness (Chanson 2010).

4 Particle trajectories

4.1 Presentation

The trajectories of fish egg substitute particles were recorded in undular and breaking tidal bores, and the flow conditions are listed in Table 1. Figure 4 presents the

instantaneous free-surface profiles for both experiments. The observations were recorded at about x = 5 m where the bore propagated upstream with a constant celerity U. The distinctive shape of the first wave length is illustrated for the undular bore experiment, with a wave period of about 0.8 s. In Figure 4, the data are presented as the dimensionless water depth d/d_o as a function of the longitudinal distance X/d_o, where d is the water depth measured above the bed and X is a longitudinal co-ordinate positive in the downstream direction. The origin of X was x = 4.85 m in Figure 4.

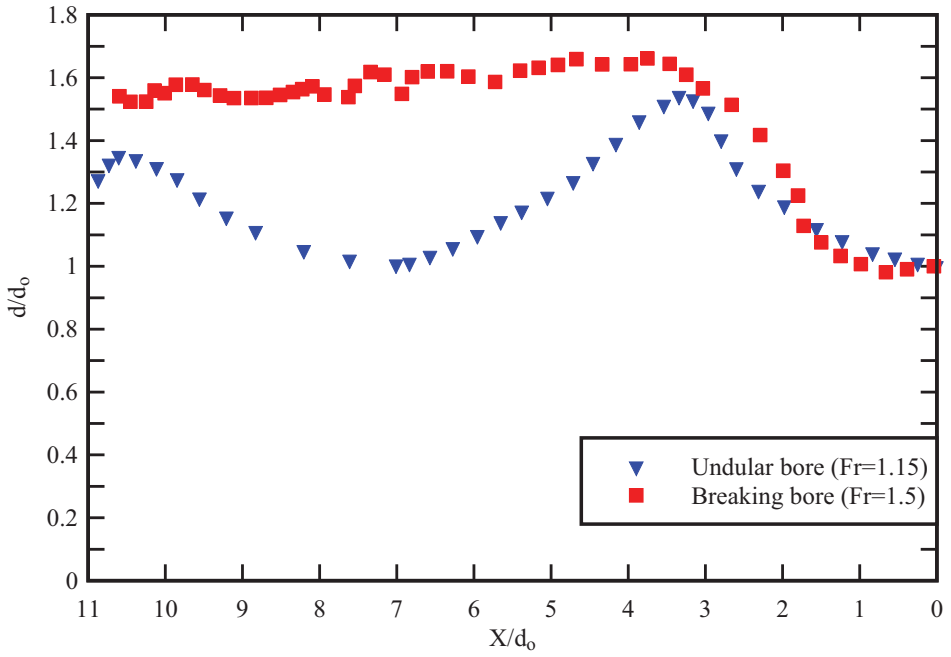

Figure 4: Dimensionless instantaneous free-surface profiles of tidal bores for the particle trajectory experiments (Q = 0.013 m^3s^{-1}, Fr = 1.15 and 1.5) - Bore propagation from left to right

Some typical particle trajectories are presented in Figures 5 and 6 for the undular and breaking tidal bores respectively. Figures 5 and 6 show some sideview of the particle trajectories. In each graph, the horizontal axis is the longitudinal coordinate x' positive downstream with x' = 0 when the particle passed beneath the leading, upstream edge of the bore front and the vertical axis is the particle vertical elevation z. Each trajectory starts at x' = 0 and the time interval between each data point is 1/30 s. In the graphs, the tidal bore propagates from left to right with x' positive to the left as in Figure 2.

In the undular bore, a range of particle trajectory patterns were observed with two distinctive trends (Fig. 5). Among the particles released in the upper flow region ($z/d_o > 0.5$), a majority followed a helicoidal pattern illustrated in Figure 5 (Particles 6a, 6c, 6d, 8b). The particles followed an orbital path beneath the wave crest when they reached a maximum elevation. Then they were advected downstream beneath the next wave trough before doing another looping beneath the next wave crest. The orbital trajectories were somehow comparable to the particle motion beneath regular wave crests (Sawaragi 1995), but the entire trajectories were a combination of orbital paths superposed to a downstream advection. When the particles were injected closer to the bed ($z/d_o < 0.5$), they were often subjected to some recirculation motion with an initially rapid deceleration followed by an upstream advection behind the bore front. For example, in Figure 5, the particles 2, 4c and 5b were recirculated upstream with a advection velocity V_x/V_o = -0.5 in average. The two distinctive trends are illustrated in Figure 5.

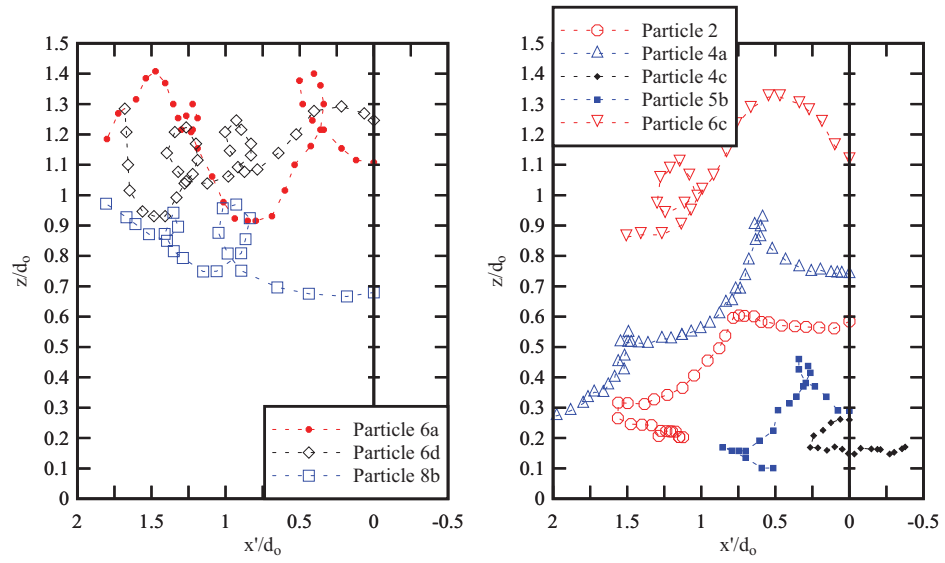

Figure 5: Dimensionless particle trajectories in the undular tidal bore (Fr = 1.15, Q = 0.013 m^3s^{-1}, d_o = 0.0775 m)

In a breaking tidal bore, the particle trajectories were more complicated (Fig. 6). Most particles that were travelling very close to the bed ($z/d_o < 0.2$) were subjected to a sudden deceleration followed by an upstream motion: e.g., the particle trajectory b8 with red circular symbols in Figure 6. The particles initially released in the upper flow region were subjected to a pseudo-chaotic motion induced by the

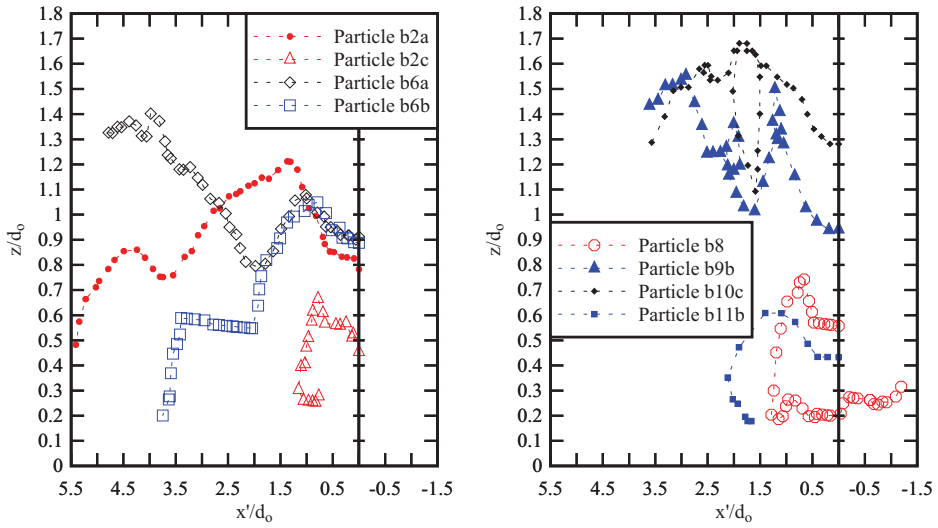

Figure 6: Dimensionless particle trajectories in the breaking tidal bore (Fr = 1.51, Q = 0.013 m^3s^{-1}, d_o = 0.0505 m)

large scale turbulent eddies generated in the mixing layer of the bore roller. Some examples of such particle trajectories are presented in Figure 6 (particles b2a, b6a, b9b, b10c).

4.2 Discussion

During the undular tidal bore experiments, the particle motion data yielded some large fluctuations of both horizontal and vertical particle velocities beneath the free-surface undulations. The long-lasting impact of the free-surface undulations is a key feature of undular tidal bores in natural systems (Koch and Chanson 2008). The comparative observations with the same initial flow rate Q suggested that the undular bore induced a greater vertical mixing of the particles compared to the breaking bore, especially in the upper flow region ($z/d_o > 0.5$). In the undular bore, the particle motion was simply influenced by the free-surface undulation pattern and the resulting streamline pattern.

5 Discussion: impact of tidal bores on fish egg turbulent dispersion

Based upon the time evolution of the particle trajectory scatter, the turbulent mixing coefficient of the particles were estimated from the mean square displacement of the particles assuming a homogenous, stationary turbulence behind the tidal bore

front:

$$\frac{D_x}{V_o d_o} = \frac{\sigma_x^2}{2\, V_o d_o\, t'} \tag{3}$$

$$\frac{D_z}{V_o d_o} = \frac{\sigma_z^2}{2\, V_o d_o\, t'} \tag{4}$$

where D_x and D_z are the turbulent mixing coefficients in the horizontal and vertical directions respectively, σ_x and σ_z are respectively the mean square displacement of the particles in the x- and z-directions, and t' is the time scale with t' = 0 when the particle passed beneath the leading edge of the bore front. Equations (3) and (4) may be derived using Langevin's model of turbulent dispersion and the random walk model assuming that t' is much larger than the Lagrangian time scale (Pope 2000). The experimental results are presented in Figure 7 where D_x and D_z characterised the turbulent mixing of the fish egg particles immediately behind the tidal bore front. Despite the simplistic assumptions underlying Equations (3) and (4), the data implied that the longitudinal mixing coefficient was nearly one order of magnitude greater than the vertical diffusion coefficient (Fig. 7), while the vertical mixing coefficient behind the tidal bores was one order of magnitude larger than the vertical diffusion coefficient in a fully-developed steady open channel flow (Fig. 7). Overall the experimental results emphasised the strong longitudinal and vertical mixing induced by the tidal bore passage, with relatively little difference between undular and breaking tidal bores.

A key feature of the present physical study is the broad range of particle trajectories and trajectory patterns beneath a tidal bore front, as well as the large-scale particle motion induced by the turbulence (Fig. 5 & 6). Both qualitative and quantitative observations suggested the existence of large scale coherent structures in which the fish egg substitutes were trapped and advected within. Earlier physical and numerical studies documented the production of such large coherent vortices (Koch and Chanson 2009, Lubin et al. 2010). These studies showed some energetic turbulent events beneath and shortly after the tidal bore front implying the generation of vorticity underneath and advected behind. The presence of the persisting turbulent vortices indicated that the tidal bore process contributed efficiently to the turbulent mixing of fish eggs and their longitudinal dispersion, thus reducing the efficiency of the predators in tidal-bore affected estuaries as proposed by Morris et al. (2003).

The present data (Fig. 5 & 6) showed some preferential dispersion of fish eggs depending upon their vertical elevation in the water column as sketched in Figure 8. The implications are discussed thereafter. In a natural estuary (Fig. 1), the fish eggs are typically advected downstream by the ebb tide. The arrival of the tidal bore does create a selective longitudinal spread of the eggs. The lightest fish eggs

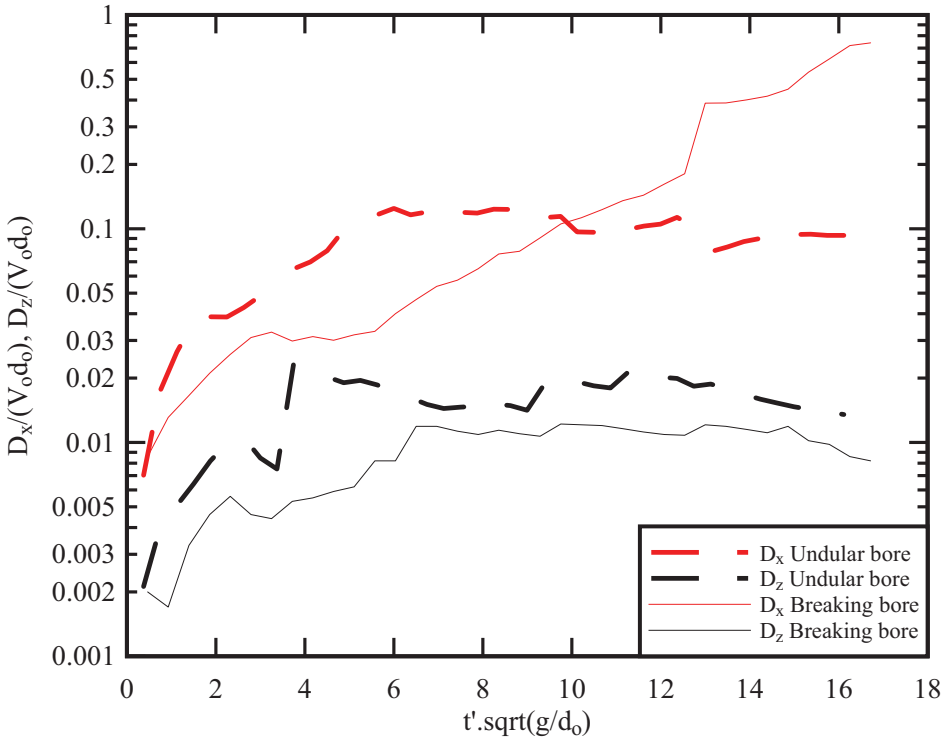

Figure 7: Dimensionless turbulent diffusion coefficients of particles in the longitudinal and vertical directions immediately behind a tidal bore front

located in the upper flow region continue to flow downstream, while the heaviest fish eggs reverse their course, flowing upstream behind the bore (Fig. 8). The tidal bore induces a very rapid longitudinal spread of the eggs with some form of preferential mixing depending upon their vertical position in the water column, hence of their density and stages of development. The heaviest, older fish eggs are advected upstream immediately after the tidal bore passage and they remain confined to the upper estuary that is the known breeding grounds of striped bass juveniles (Rulifson and Tull 1999, Morris et al. 2003). The lightest, neutrally buoyant eggs located next to the surface continue their journey downstream possibly up to the river mouth, although the strong flood flow may bring them back into the upper estuary at a later stage of the tidal cycle. Figure 8 illustrates the preferential/selective dispersion of fish eggs under a tidal bore.

Lastly note the limitations of the present investigation. The experimental study was focused on centreline measurements implying a two-dimensional flow motion. Some qualitative tests were conducted by placing a camera above the channel. The

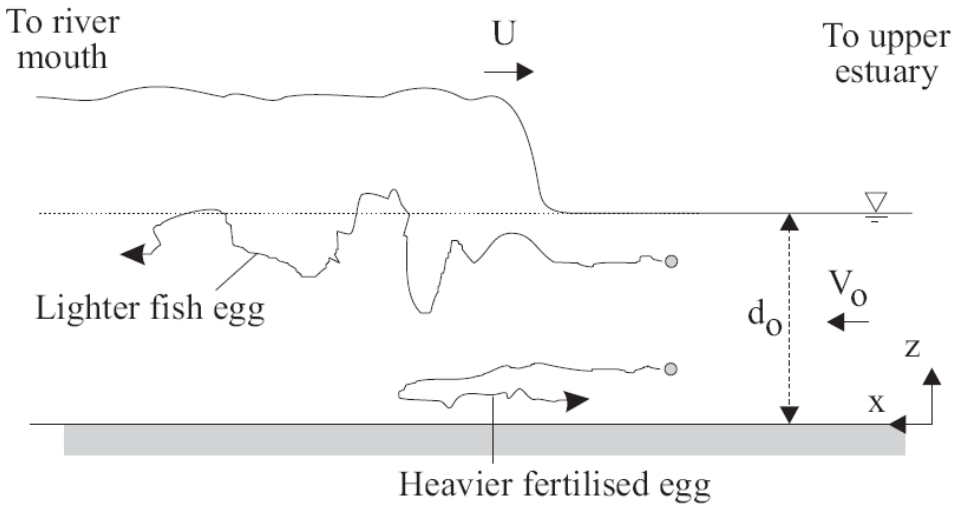

Figure 8: Sketch of selective dispersion of fish eggs beneath a tidal bore

observations indicated that the particles remained qualitatively along the channel centreline, but the visual observations were adversely affected by the free-surface turbulence during and immediately after the bore front propagation. Newer experiments could be conducted using a transparent channel bed, but the technique would only apply to a smooth channel bed. In most natural systems, the estuarine channel is comparatively wider, and the tidal bore motion may be three-dimensional. This feature may have some impact on the fish egg longitudinal and transverse dispersion.

6 Conclusion

This physical study focused on the turbulent dispersion of fish egg-like particles beneath a tidal bore. Experimental measurements were performed with small particles whose properties were close to those of striped bass (*Morone saxatilis*) fish eggs , and their turbulent dispersion associated with the passage of undular and breaking bores was documented.

The findings were consistent with some earlier experimental and numerical results, including the observations of rapid flow deceleration and flow reversal beneath the breaking bore roller. Some seminal features were highlighted, including some large-scale motion implying the existence of large coherent structures. These large turbulent eddies are responsible for some bed erosion and vertical mixing of the water column when a tidal bore propagates upstream in the estuarine zone of a natural system. The large-scale vortices are also responsible to the longitudinal

dispersion of fish eggs reducing the impact of predators, although the present findings highlighted some form of preferential dispersion patterns depending upon the vertical elevation of fish eggs within the water column, and hence their density and development stages.

Finally it must be noted that the present experiments were performed with an unique particle size and density. Future tests should encompass a range of particle sizes and density.

Acknowledgement: The first author thanks Dr Roger Rulifson (East Carolina University) for his helpful comments. The authors acknowledge the technical assistance of Graham Illidge and Clive Booth (The University of Queensland).

References

Benet, F., Cunge, J.A. (1971): Analysis of Experiments on Secondary Undulations caused by Surge Waves in Trapezoidal Channels. *Journal of Hydraulic Research*, IAHR, vol. 9, no. 1, pp. 11-33.

British Standard (1943): Flow Measurement. British Standard Code BS 1042:1943, British Standard Institution, London.

Chanson, H. (2011): Current Knowledge in Tidal bores and their Environmental, Ecological and Cultural Impacts. *Environmental Fluid Mechanics*, vol. 11, no. 1, pp. 77-98 (DOI: 10.1007/s10652-009-9160-5).

Chanson, H. (2010): Unsteady Turbulence in Tidal Bores: the Effects of Bed Roughness. *Journal of Waterway, Port, Coastal, and Ocean Engineering, ASCE,* vol. 136, no. 5, pp. 247-256 (DOI: 10.1061/(ASCE)WW.1943-5460.0000048).

Favre, H. (1935): Etude Théorique et Expérimentale des Ondes de Translation dans les Canaux Découverts. Dunod, Paris, France.

Hornung, H.G., Willert, C., Turner, S. (1995): The Flow Field Downstream of a Hydraulic Jump. *Journal of Fluid Mech.*, vol. 287, pp. 299-316.

Koch, C., Chanson, H. (2008): Turbulent Mixing beneath an Undular Bore Front. *Journal of Coastal Research*, vol. 24, no. 4, pp. 999-1007 (DOI: 10.2112/06-0688.1).

Koch, C., Chanson, H. (2009): Turbulence Measurements in Positive Surges and Bores. *Journal of Hydraulic Research*, IAHR, vol. 47, no. 1, pp. 29-40 (DOI: 10.3826/jhr.2009.2954).

Lighthill, J. (1978): Waves in Fluids, Cambridge University Press, Cambridge, UK, 504 pages.

Lubin, P., Glockner, S., Chanson, H. (2010): Numerical Simulation of a Weak

Breaking Tidal Bore. *Mechanics Research Communications*, vol. 37, no. 1, pp. 119-121 (DOI: 10.1016/j.mechrescom.2009.09.008).

Morris, J.A., Rulifson, R.A., Toburen, L.H. (2003): Life History Strategies of Striped Bass, Morone Saxatilis, Populations inferred from Otolith Microchemistry. *Fisheries Research*, vol. 62, pp. 53-63.

Pope, S.B. (2000): Turbulent Flows, Cambridge University Press, 771 pages.

Rulifson, R.A., Tull, K.A. (1999): Striped Bass Spawning in a Tidal Bore River: the Shubenacadie Estuary, Atlantic Canada. *Transactions of the American Fisheries Society*, vol. 128, pp. 613-624.

Sawaragi, T. (1995): Coastal Engineering - Waves, Beaches, Wave-Structure Interactions. Elsevier, Developments in Geotechnical Engineering Series, no. 78, Amsterdam, The Netherlands, 479 pages.

Simpson, J.H., Fisher, N.R., Wiles, P. (2004): Reynolds Stress and TKE Production in an Estuary with a Tidal Bore. Estuarine, *Coastal and Shelf Science*, vol. 60, no. 4, pp. 619-627.

Treske, A. (1994): Undular Bores (Favre-Waves) in Open Channels - Experimental Studies. *Journal of Hydraulic Research*, IAHR, vol. 32, no. 3, pp. 355-370.

Tull, K.A. (1997): Spawning Activity of triped Bass in a Tidal Bore River: the Shubenacadie-Stewiacke System, Nova Scotia. M.Sc. thesis, University of East Carolina, Dept of Biology, 140 pages.

Wolanski, E., Williams, D., Spagnol, S., Chanson, H. (2004): Undular Tidal Bore Dynamics in the Daly Estuary, Northern Australia. Estuarine, *Coastal and Shelf Science*, vol. 60, no. 4, pp. 629-636.